Neutral-ionic interface in organic charge-transfer salts

Z. G. Soos and S. Mazumdar
Department of Chemistry, Princeton University, Princeton, New Jersey 08540
(Received 30 March 1978)

Charge transfer (CT) stabilization in linear stacks $\ldots D^{\gamma+}A^{\gamma-}D^{\gamma+}A^{\gamma-}\ldots$ of π-electron donors (D) and acceptors (A) involve spin-dependent configuration interactions that are treated exactly in rings of $N = 4$, 6, 8, 10 sites, and extrapolated to $N \to \infty$, by adapting valence-bond techniques to electron-hole excitations. The ground state CT $\gamma(z)$ and the magnetic gap $\Delta E_m(z)/\sqrt{2}|t|$ to the lowest triplet are computed for arbitrary $z = \delta/\sqrt{2}|t|$, where -2δ is the energy for $DA \to D^+A^-$, $-|t| = \langle D^+A^-|\mathcal{H}|DA\rangle$ is the Mulliken CT integral, and D^{2+}, A^{2-} sites are excluded. The spin degeneracy of $A^-\sigma$ and $D^+\sigma$ ion radicals is treated exactly. Instead of the discontinuous change from $\gamma = 0$ to $\gamma = 1$ in the limit $|t| \to 0$, finite overlap gives a continuous $\gamma(z)$ and $\gamma(z_c) = 0.68 \pm 0.01$ at the neutral-ionic interface $z_c = 0.53 \pm 0.01$. The magnetic gap ΔE_m is finite for $z < z_c$ and vanishes for $z \geq z_c$, where there is a diamagnetic to paramagnetic transition and the ground state switches from $k = 0$ to $k = \pi$ symmetry. Collective effects due to long-range three-dimensional Coulomb interactions are included in a Hartree approximation and produce a first-order transition, with discontinuous $\gamma(z)$, when the critical value $m/\sqrt{2}|t| = 1.4 \pm 0.1$ of the Madelung stabilization m of a dimer is exceeded. The puzzling magnetic gaps in paramagnetic organic CT salts with mixed regular stacks arise naturally for partial CT and $z < z_c$. Valence-bond analysis of CT excitations models the physical properties of organic complexes with overlapping sites and intermediate γ.

I. INTRODUCTION

Ionic lattices are formed when the Madelung energy M per ion pair exceeds the energy $I_D - A_A$ of transferring an electron from a donor (D) to an acceptor (A). NaCl is an elementary example in which D = Na, A = Cl produces a lattice based on closed-shell, diamagnetic Na^+ and Cl^- ions. Alkaline-earth oxides approximate divalent ionic lattices, in spite of the large energy needed to transfer a second electron. Strong organic donors and acceptors[1] also crystallize as salts when M exceeds $I_D - A_A$. Now D and A are closed-shell π-electron molecules and paramagnetism is associated with the $s = \frac{1}{2}$ ion radicals D^+ and A^-. In the limit of nonoverlapping sites, an integral number of electrons can be associated with each lattice site. Both organic and inorganic salts then show sharp neutral-ionic interfaces, with $D^{\gamma+}A^{\gamma-}$ lattices that are either neutral ($\gamma = 0$) or ionic ($\gamma = 1$). The simple condition $M > I_D - A_A$ for an ionic lattice can readily be generalized to include all intermolecular interactions of both the neutral and the ionic lattice.

Real solids have overlapping sites, with nonvanishing Mulliken charge transfer (CT) integral $t = -|t|$:

$$t = \langle D^+A^-|\mathcal{H}|DA\rangle. \tag{1}$$

CT interactions can be generalized[2] to crystal-perturbed states. In organic solids based on planar aromatic donors and acceptors, overlap is largely restricted to one-dimensional stacks on the basis of the polarization of the CT absorption and the great anisotropy of electric and magnetic properties.[3] A sharp neutral-ionic interface clearly requires that t, which is of the order of 0.1–0.3 eV, be far smaller than $M - (I_D - A_A)$, which is about -4 to $+2$ eV. Borderline cases with $t \sim |M - (I_D - A_A)|$ have nonintegral γ in the ground electronic state.[4]

We present in this paper the first exact analysis of the neutral-ionic interface for overlapping sites.[5] The ground-state CT, γ, of the one-dimensional stack $\ldots D^{\gamma+}A^{\gamma-}D^{\gamma+}A^{\gamma-}\ldots$ is found as a function of $\delta/\sqrt{2}|t|$ where -2δ is the energy required to transfer an electron from D to A in the partly ionized solid. The energy ΔE_m of the lowest triplet above the singlet ground state is also computed and plays a central role in the magnetic properties. ΔE_m is finite for a neutral lattice and vanishes for $\gamma > \gamma_c \simeq 0.68 \pm 0.01$, where a diamagnetic to paramagnetic transition occurs at 0 °K.

Overlapping sites necessarily require a many-body approach and idealized models. We nevertheless can include the key physical features of correlations in narrow-band solids and of collective effects due to the long-range Coulomb interactions of the ionic solid. The collective nature of the neutral-ionic transition arises because it is easier to transfer electrons in an almost ionic lattice, with Madelung energy $M\gamma^2$ per pair, than in a neutral lattice, where only the nearest-neighbor interaction M_1 stabilizes the D^+A^- ion pair. In the Hartree approximation[1,3] for the long-range, three-dimensional Coulomb interactions, the energy -2δ

for transferring an electron from D to A depends on γ:

$$\delta(\gamma) = \delta(0) + m\gamma. \tag{2}$$

For a neutral ($\gamma = 0$) lattice, $-2\delta(0)$ is approximately

$$-2\delta(0) \equiv E(D^+A^-) - E(DA) \simeq I_D - A_A - M_1. \tag{3}$$

The charge distributions of D^+ and A^- at the crystal separation leads to $M_1 \sim 4$ eV in organic CT complexes.[6] Embedding the dimer in the solid yields[7] the additional stabilization $m = M - M_1 \sim 1$ eV favoring an ionic lattice. Thus $-2\delta(\gamma)$ in (2) vanishes at $\gamma = \frac{1}{2}$ for $M = I_D - A_A$, the usual interface between the neutral and ionic lattice, and energy is gained thereafter on further ionization.

The neutral-ionic interface in organic solids involves $\gamma \simeq 0$ and $\gamma \simeq 1$. Doubly ionized D^{2+} or A^{2-} sites are energetically quite unfavorable. Our model overestimates such electron-electron correlations by excluding D^{2+} or A^{2-} sites. Each donor can then be in the three cyrstal perturbed electronic states, D, $D^+\alpha$, and $D^+\beta$; each acceptor in A, $A^-\alpha, A^-\beta$. The enumeration of all possible charge and spin distributions for a chain of N sites formally resembles a valence-bond (VB) description[8] of π electrons. The size of the basis set increases as 3^N and is only slightly reduced by application of charge conservation and symmetry. Overlapping sites lead to linear combinations of these VB basis states in which any site can occur with different charge or spin, thus producing a nonintegral ground-state CT γ. The interplay between the CT integral $t = -|t|$ in (1) for nearest-neighbor transfers along the DA stack and the energy -2δ in (2) for producing a D^+A^- pair is treated exactly for rings up to $N = 10$ in terms of the single parameter $z = \delta/\sqrt{2}\,|t|$.

Section II develops a model for the neutral-ionic interface in terms of an electron-hole representation whose diagrammatic analysis by VB methods is the principal mathematical result of the paper. This method can be applied to other topologies, although a one-dimensional system yields by far the simplest $N \to \infty$ extrapolations. The inclusion of collective effects in $\delta(\gamma)$ and the behavior of $\gamma(z)$ and $\Delta E_m(z)$ are discussed in Sec. III. The neutral-ionic interface is not symmetric about $z = 0$ on account of the different spin degeneracies of neutral and ionic sites. The lattice at 0 °K undergoes a diamagnetic to paramagnetic transition at $z_c = 0.53 \pm 0.01$, which is computed here for the first time. The fact that $\Delta E_m(z)$ does not vanish for $z < z_c$ even in regular lattices with a single CT integral offers a natural explanation for the static susceptibilities of several solid organic CT complexes. These ionic solids can now be described as showing partial CT, thus removing the fundamental theoretical difficulties of models based on $\gamma \sim 1$.

II. VALENCE-BOND ANALYSIS OF ELECTRON-HOLE EXCITATIONS

The molecular sites in the one-dimensional array $\ldots D^{\gamma+}A^{\gamma-}D^{\gamma+}A^{\gamma-}\ldots$ are labeled consecutively, with odd n for D sites and even n for A sites. The electron-hole vacuum $|0\rangle$ is defined as the neutral lattice $|\ldots DADA\ldots\rangle$ and is represented by N points for N sites. Fermi creation operators $c^\dagger_{n\sigma}$ create a crystal perturbed $A^-\sigma$ state for even n and a $D^+\sigma$ state for odd n. The CT excitation for a DA dimer is induced by the operator

$$(n,n+1)^\dagger \equiv 2^{-1/2}(c^\dagger_{n\alpha}c^\dagger_{n+1\,\beta} + c^\dagger_{n\beta}c^\dagger_{n+1\,\alpha}), \tag{4}$$

which is denoted as an arrow from n to $n+1$. It can be verified directly that $(n,n+1)^\dagger|0\rangle$ is a normalized singlet state in which sites n and $n+1$ have an electron-hole excitation corresponding to transferring an electron from D to A. The matrix element of $\mathcal{H}$ between $|0\rangle$ and $(n,n+1)^\dagger|0\rangle$ is just $\sqrt{2}t$. Reversing the arrow, or bond, gives

$$(n+1,n)^\dagger = -(n,n+1)^\dagger, \tag{5}$$

since two Fermi operators are interchanged in (4). The adjoint operator $(n+1,n)$ returns $(n,n+1)^\dagger|0\rangle$ to the vacuum $|0\rangle$.

Any charge and spin distribution on the one-dimensional lattice can be represented diagrammatically by points for neutral sites, by arrows for singlet-correlated D^+A^- sites, and by notched arrows for triplet-correlated D^+A^- sites. The exclusion of D^{2+} and A^{2-} sites means that no VB structure has two arrows at any site. Charge conservation requires equal numbers of electron excitations (A^- sites) and hole excitations (D^+ sites),

$$\sum_{\substack{n\sigma \\ \text{even}}} c^\dagger_{n\sigma}c_{n\sigma} = \sum_{\substack{n\sigma \\ \text{odd}}} c^\dagger_{n\sigma}c_{n\sigma}. \tag{6}$$

The dimension of the VB basis for N sites can be computed by noting that there are $\binom{N/2}{p}$ ways of ionizing p of the $N/2$ D sites and $\binom{N/2}{p}$ ways of distributing p A^- sites to satisfy (6). Since the spin degeneracy of $A^-\sigma$ or $D^+\sigma$ is 2, that of p ionic pairs is 2^{2p}, and the total number of VB structures is

$$N_T = \sum_{p=0}^{N/2} \binom{N/2}{p}^2 2^{2p}. \tag{7}$$

N_T is listed in Table I for $N = 4$, 6 8, and 10, which is the largest ring considered.

The electron-hole representation of a mixed DA stack with D^{2+} and A^{2-} sites excluded, with nearest-neighbor CT integrals $t = -|t|$, and with energy -2δ for transferring an electron from D to A thus leads to the basic equation of our model,

TABLE I. Dimensions N_T of the VB basis set and M of selected subspaces of $\mathcal{H}_0$ with fixed S and k for a ring of N sites.

Ring N	VB Basis N_T, Eq. (7)	Singlets ($S=0$) Total	$M(k=0)$	$M(k=\pi)$	Triplets ($S=1, M_s=1$) Total	$M(k=\pi)$
4	33	7	3	2	7	2
6	245	30	6	6	42	7
8	1 921	143	19	17	296	27
10	15 525	708	73	75	1475	98

$$\mathcal{H}_0 = -\sqrt{2}\,|t| \times\left(z\sum_{n\sigma} c^\dagger_{n\sigma}c_{n\sigma} + \sum_n [(n,n+1)^\dagger + (n+1,n)]\right), \quad (8)$$

with $z = \delta/\sqrt{2}\,|t|$. Since CT does not involve spin flips, the total spin S is conserved and only singlet operators $(n,n+1)^\dagger$ and $(n+1,n)$ occur. Furthermore, the C_N rotational symmetry of a ring of N sites allows the classification of the eigenstates of $\mathcal{H}_0$ by the wave vector k,

$$k = 0,\ \pm 2\pi/N,\ \pm 4\pi/N, \ldots, +\pi. \quad (9)$$

The dimensions of several exact subspaces $\{S,k\}$ of $-\mathcal{H}_0/\sqrt{2}\,|t|$ for rings with $N=4$, 6, 8, and 10 sites are listed in Table I. The VB analysis of $-\mathcal{H}_0/\sqrt{2}\,|t|$ in these exact subspaces is developed below.

Several qualitative features of $\mathcal{H}_0$ follow directly: $z \to -\infty$ corresponds to $\gamma = 0$, since creating an electron-hole pair costs $-\sqrt{2}\,|t|z = |\delta|$, while $z \to +\infty$ yields $\gamma = 1$, with all sites ionic, and $z \sim 0$ describes comparable values of t and δ around the neutral-ionic interface. Other properties of $\mathcal{H}_0$ can be obtained from the generalization

$$\mathcal{H}_{eh} = \mathcal{H}_0 + U\sum_n c^\dagger_{n\alpha}c^\dagger_{n\beta}c_{n\beta}c_{n\alpha}, \quad (10)$$

where $U>0$ is the correlation energy for creating D^{2+} states at odd n and A^{2-} states at even n. The $U \to \infty$ limit of the electron-hole Hubbard model (10) excludes doubly ionized sites and reduces to $\mathcal{H}_0$. The canonical transformation $c^\dagger_{n\sigma} \to a_{n\sigma}$ for odd n and $c_{n\sigma} \to a_{n\sigma}$ for even n leads to the modified Hubbard model[4,7]

$$\mathcal{H}_{\rm mod} = \sum_{\substack{n\sigma \\ \text{even}}} \epsilon_A a^\dagger_{n\sigma}a_{n\sigma} + \sum_{\substack{n\sigma \\ \text{odd}}} \epsilon_D a^\dagger_{n\sigma}a_{n\sigma} + t\sum_{n\sigma}(a^\dagger_{n\sigma}a_{n+1\,\sigma} + a^\dagger_{n+1\,\sigma}a_{n\sigma}) + U\sum_n a^\dagger_{n\alpha}a^\dagger_{n\beta}a_{n\beta}a_{n\alpha}, \quad (11)$$

where we have neglected the additive constant $(2\epsilon_D + U)N/2$ associated with the neutral lattice $|0\rangle$. The highest occupied molecular orbital (HOMO) energy $\epsilon_D = +\delta - U$ of D sites and the lowest unoccupied molecular orbital (LUMO) energy $\epsilon_A = -\delta$ of A sites are shown in Fig. 1, together with the on-site correlation $U>0$ for doubly occupying D sites in the electron-hole vacuum or A^{2-} sites. The self-consistent solution[4] of (10) for N electrons on N sites is an approximate solution of $\mathcal{H}_{eh}$ for finite U. Long-range Coulomb interactions can be included,[9] in a Hartree approximation, by redefining the coefficients ϵ_A, ϵ_D, and U in (11). An energy gap for optical transitions is found[9] even at the neutral-ionic interface, but magnetic properties are spoiled in self-consistent solutions.[4] Since $\mathcal{H}_0$ is the $U \to \infty$ limit of a Hubbard model, it conserves the total spin S and has its absolute ground state in the $S=0$ subspace. The lowest magnetic excitation is a triplet ($S=1$) state with energy ΔE_m.

The ground-state properties of $\mathcal{H}_0$ in (8) are thus associated with the $S=0$ subspace. The ground

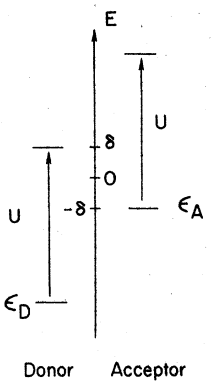

FIG. 1. Schematic representation of the energy levels ϵ_D for D sites and ϵ_A for A sites, with the correlation energy U for doubly occupying either ϵ_D or ϵ_A. The energy for the electron transfer DA to D^+A^- is -2δ.

state is nondegenerate and is consequently in either the $k=0$ or $k=\pi$ subspaces listed in Table I for rings of up to $N=10$. The vacuum state $|0\rangle$ clearly transforms as $k=0$ and is the ground state in the limit $z\to-\infty$ of a neutral lattice. The fully ionic lattice $\ldots D^+A^-D^+A^-\ldots$ has a charge-density wave and transforms as $k=\pi$, with a change in phase for every rotation of $2\pi/N$. Thus the absolute ground state is in $\{0,0\}$ for $z<z_c(N)$ and in $\{0,\pi\}$ for $z>z_c(N)$. The average degree of CT γ is just the average number of electron-hole excitations in the absolute ground state,

$$\gamma(z,N)=\frac{1}{N}\left\langle\sum_{n\sigma}c^\dagger_{n\sigma}c_{n\sigma}\right\rangle=-\frac{\partial}{\partial z}\langle\mathcal{H}_0\rangle/\sqrt{2}\,|t|N. \quad (12)$$

Numerical differentiation of the lowest $S=0$ eigenvalue of $\mathcal{H}_0$ for a given ring N thus yields γ directly. The crossover region $z_c(N)$ from $k=0$ to $k=\pi$ involves a change of slope, or a jump in γ, and defines the neutral-ionic interface.

Arranging the sites in a ring minimizes end effects. The VB analysis of $-\mathcal{H}_0/\sqrt{2}\,|t|$ for $N=6$, the "benzene" case in the Rumer-Pauling method,[8] will now be summarized. The extension to larger N is straightforward. The vacuum state $|0\rangle$ is represented in Fig. 2 by the six points of a hexagon. The VB ket $|1\rangle$:

$$|1\rangle=\sum_n(n,n+1)^\dagger|0\rangle\ , \quad (13)$$

from Fig. 2 is clearly the $k=0$ linear combination of VB structures with one bond, a singlet-correlated electron-hole represented by an arrow from n to $n+1$. Remembering that the exclusion of D^{2+} or A^{2-} sites implies that each site has at most a single bond, we see that another application of $-\mathcal{H}_0/\sqrt{2}\,|t|$ produces the two VB structures $|3\rangle$ and $|4\rangle$ in Fig. 2. The singlet annihilation operators

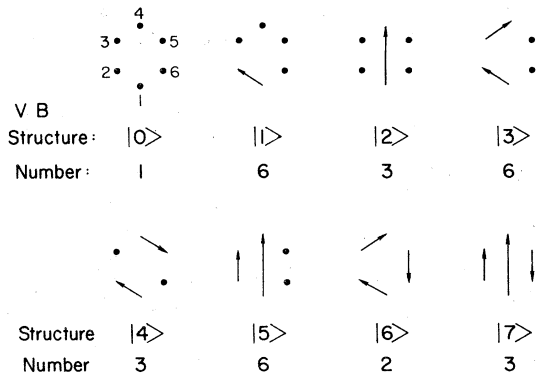

FIG. 2. Valence-bond structures in the singlet subspace of $\mathcal{H}_0$, Eq. (8), for a ring with $N=6$ sites. Donors occupy the odd sites and acceptors the even sites.

in $-\mathcal{H}_0/\sqrt{2}\,|t|$ acting on $|3\rangle$ induce long-bonded structures such as $|2\rangle$, as can be verified from the general identity

$$(n+2,n+1)(n,n+1)^\dagger(n+2,n+3)^\dagger=\tfrac{1}{2}(n,n+3)^\dagger. \quad (14)$$

Since interchanging the sense of a bond changes sign, as shown in (5), the $k=0$ linear combination of long-bonded singlets vanishes.

Repeated application of $h=-\mathcal{H}_0/\sqrt{2}\,|t|$ interrelates the VB kets in Fig. 2. The resulting linear equations in the $S=0, k=0$ subspace are

$$\begin{aligned}
&h|0\rangle=|1\rangle\ ,\\
&h|1\rangle=2z|1\rangle+6|0\rangle+2|3\rangle+2|4\rangle\ ,\\
&h|3\rangle=4z|3\rangle+2|1\rangle+3|6\rangle\ ,\\
&h|4\rangle=4z|4\rangle+|1\rangle\ ,\\
&h|5\rangle=4z|5\rangle+|1\rangle\ ,\\
&h|6\rangle=6z|6\rangle+|3\rangle-\tfrac{1}{2}|5\rangle\ .
\end{aligned} \quad (15)$$

The fully ionic structures $|6\rangle$ and $|7\rangle$ are the usual[8] neutral VB kets for benzene and describe the different ways of spin-pairing a single electron at each site. The present interpretation is quite different physically: the Kekulé structures $|6\rangle$ and Dewar structures $|7\rangle$ have the same energy $6z$ under the diagonal part of $-\mathcal{H}_0/\sqrt{2}\,|t|$, which merely counts the number of ionic sites. However the mathematical results[8] for the completeness of the VB basis, for evaluating overlaps between structures, and for finding linearly independent structures are directly applicable to $\mathcal{H}_0$. For example, VB structures with intersecting bonds are not linearly independent and need not be included in Fig. 2.

The linear equations (15) describe exactly the configuration interaction of all $S=0, k=0$ linear combinations of VB structures in Fig. 2. To obtain nontrivial solutions for the eigenvalues, we arrange the coefficient in columns to form a matrix

$$\frac{-\mathcal{H}_0}{\sqrt{2}\,|t|}=\begin{bmatrix}
0 & 6 & 0 & 0 & 0 & 0\\
1 & 2z & 2 & 1 & 1 & 0\\
0 & 2 & 4z & 0 & 0 & 1\\
0 & 2 & 0 & 4z & 0 & 0\\
0 & 0 & 0 & 0 & 4z & -1/2\\
0 & 0 & 3 & 0 & 0 & 6z
\end{bmatrix} \quad (16)$$

and find the roots of the corresponding determinant. Since the convenient VB basis $|0\rangle$, $|1\rangle$, $|3\rangle$, $|4\rangle$, $|5\rangle$, and $|6\rangle$ in $\{0,0\}$ is neither normal nor

orthogonal, (16) is not symmetric. It can be symmetrized by orthonormalizing the basis, but such a procedure is tedious for the large M values of symmetry-adapted states listed in Table I for $N=8$ or 10. The *largest* eigenvalue $\lambda_{00}(z)$ of (16) gives the exact ground-state energy $-\sqrt{2}\,|t\,|\lambda_{00}(z)$ in the $\{0,0\}$ subspace of $\mathcal{H}_0$. This root and the corresponding eigenvector are readily obtained[10] iteratively from (16). We start with a normalized M-component vector each of whose elements is $M^{-1/2}$, multiply by (16), normalize the resulting vector, and repeat until the eigenvalue λ_{00} and eigenvector cease changing. Varying z in (16) is straightforward, since the energy $-\sqrt{2}\,|t\,|z=2\delta$ of D^+A^- pairs only occurs on the diagonal. Thus $\lambda_{00}(z)$ and its numerical derivative leading to γ are readily found.

Each rotation of $2\pi/N$ changes the phase in the $k=\pi$ linear combinations of the VB structures in Fig. 2. We take positive phases for $(n,n+1)^\dagger$ bonds when n is odd and negative phases when n is even. Thus $|1\rangle$ in (13) now has a phase factor of $(-1)^{n+1}$. Configuration interaction in the $\{0,\pi\}$ subspace of $h=-\mathcal{H}_0/\sqrt{2}\,|t\,|$ interrelates $|1\rangle$, $|2\rangle$, $|3\rangle$, $|5\rangle$, $|6\rangle$, and $|7\rangle$:

$$
\begin{aligned}
h\,|1\rangle &= 2z\,|1\rangle + 2\,|3\rangle\,,\\
h\,|2\rangle &= 2z\,|2\rangle + |5\rangle\,,\\
h\,|3\rangle &= 4z\,|3\rangle + 2\,|1\rangle + |3\rangle + 3\,|6\rangle\,,\\
h\,|5\rangle &= 4z\,|5\rangle + |1\rangle + 2\,|3\rangle + 2\,|7\rangle\,,\\
h\,|6\rangle &= 6z\,|6\rangle + |3\rangle + \tfrac{1}{2}\,|5\rangle\,,\\
h\,|7\rangle &= 6z\,|7\rangle + |3\rangle + |5\rangle\,.
\end{aligned}
\tag{17}
$$

The neutral state $|0\rangle$ and the state $|4\rangle$ vanish, while long-bonded kets based on $|2\rangle$ and $|7\rangle$ contribute. Arranging the coefficients of (17) in columns again generates a nonsymmetric 6×6 determinant whose largest root $\lambda_{0\pi}(z)$ gives the exact ground-state energy $-\sqrt{2}\,|t\,|\lambda_{0\pi}(z)$ in the $\{0,\pi\}$ subspace of $\mathcal{H}_0$.

It is clear that $k=\pi$ favors the ionic side, since both of the fully-ionized VB structures $|6\rangle$ and $|7\rangle$ in Fig. 2 contribute, while the vacuum state $|0\rangle$ does not. Indeed, all $k=\pi$ subspaces have at least one ionpair and, for a ring of N sites, have $\gamma(z)\to 2/N$ in the limit $z\to-\infty$. The crossover from $\lambda_{00}(z)$ to $\lambda_{0\pi}(z)$ as the absolute ground state occurs at $z_c(N)=0.415$ for $N=6$. The change in slope from $\lambda'_{00}(z)/N$ for $z\le z_c$ to $\lambda'_{0\pi}(z)/N$ for $z>z_c$ is shown in Fig. 3 for $N=4,6,8,10$. In the limit $N\to\infty$, the occurrence of at least one ion pair in the $k=\pi$ subspace cannot change the energy per site and $\gamma(z)$ has a point of inflection, instead of a discontinuity, at z_c. Extrapolating the discontinuity of $\Delta\gamma$ at $z_c(N)$ in Fig. 3 gives $z_c=0.52\pm0.01$.

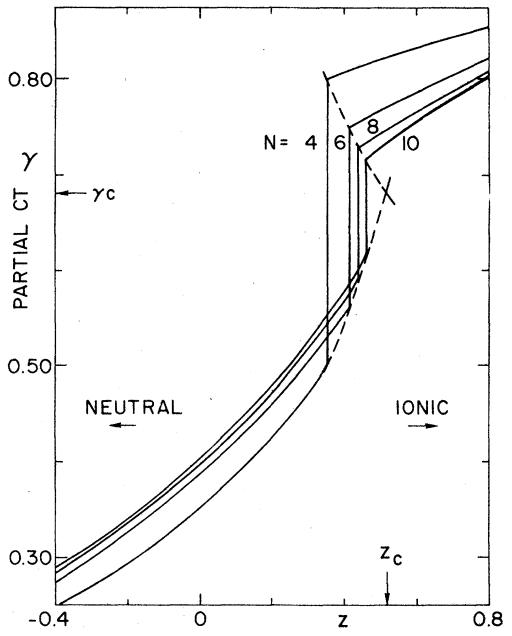

FIG. 3. Degree of CT $\gamma(z,N)$ in the singlet ground state of rings of $N=4$, 6, 8, 10 sites as a function of $z=\delta/\sqrt{2}\,|t\,|$. The crossover $z_c(N)$ from $k=0$ to $k=\pi$ symmetry results in a discontinuity for finite N and a point of inflection at z_c in the limit $N\to\infty$.

Table II lists the absolute singlet energies per sites and $\gamma(z,N)$ for representative z values at $N=4,6,8,10$. The numerical derivative in (12) gives the degree of CT $\gamma(z,N)$ in Fig. 3 while $z_c(N)$ is the crossover from the $k=0$ to the $k=\pi$ singlet ground state. The rapid convergence of $-\lambda_0/N$ as approximately N^{-4} is the basis for the $N\to\infty$ extrapolations in Table II, while the N^{-1} plot of $z_c(N)$ in Fig. 4 yields the second estimate $z_c=0.53\pm0.01$.

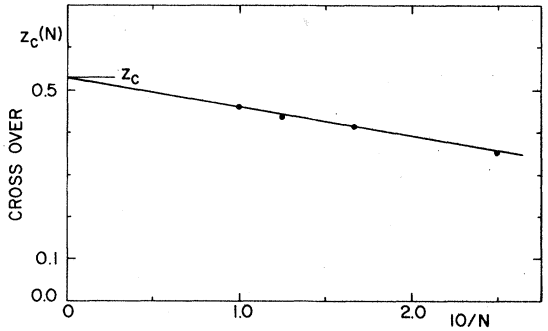

FIG. 4. Crossover $z_c(N)$ from a $k=0$ to a $k=\pi$ absolute ground state for rings with $N=4$, 6, 8, 10 sites. The linear extrapolation against N^{-1} gives $z_c=0.53\pm0.01$.

TABLE II. Absolute ground-state energy $\lambda_0(z)/N$, in units of $-\sqrt{2}t$, and degree of CT $\gamma(z)$ of $\mathcal{H}_0$, Eq. (8), for rings of $N=4,6,8,10$ sites.

$z=\delta/\sqrt{2}\,\lvert t\rvert$		Ring size N 4	6	8	10	Extrapolation [a] ∞
0.8	$\lambda_0 N^{-1}$	1.076 970	1.095 203	1.097 644	1.096 973	1.097 0
	γ	0.854 8	0.820 1	0.807 5	0.802 7	0.792
0.4	$\lambda_0 N^{-1}$	0.744 410	0.784 146	0.797 226	0.802 022	0.811 0
	γ	0.806 2	0.553 8	0.568 3	0.579 7	0.612
0.0	$\lambda_0 N^{-1}$	0.559 020	0.598 767	0.606 669	0.608 912	0.610 5
	γ	0.350 6	0.386 1	0.398 5	0.403 0	0.415
−0.4	$\lambda_0 N^{-1}$	0.441 096	0.467 390	0.471 315	0.472 279	0.474 8
	γ	0.248 3	0.277 1	0.285 5	0.287 6	0.292
−0.8	$\lambda_0 N^{-1}$	0.356 109	0.372 532	0.374 299	0.374 735	0.375 7
	γ	0.181 4	0.201 1	0.204 7	0.207 5	0.209 2
	$z_c(N)$ [b]	0.354	0.415	0.438	0.462	0.53 ± 0.01

[a] ±0.0005 for $\lambda_0 N^{-1}$, ±0.002 for γ.
[b] Crossover from $k=0$ to $k=\pi$ absolute ground state.

The VB procedure allows the matrix elements of $-\mathcal{H}_0/\sqrt{2}\,\lvert t\rvert$ to be generated almost by inspection in terms of symmetry-adapted kets. Even the $N=10$ subspaces involve only some hours, although higher N is likely to be prohibitive in view of the increasing dimensions suggested by the data in Table I. The iterative solution[10] of the largest eigenvalue of the M-dimensional subspaces is fast and economical, involving less than 2 sec of IBM 360/91 time per subspace for $N \leq 8$ and about 20 and 40 sec, respectively, for $S=0$ and $S=1$ subspaces for $N=10$. The numerical analysis is facilitated by adding a number like 10 to the diagonal elements of (16), thereby shifting all energy levels and ensuring that the matrices are not singular for any z values of interest.

Since $\lvert 0\rangle$ is necessarily a singlet, the most neutral triplet-correlated electron-hole pairs for $N=6$ are the VB structures $\lvert 1\rangle$ and $\lvert 2\rangle$ in Fig. 5. The $M_s=1,0,-1$ components of a triplet are induced by the operator

$$(n,n+1)_T^\dagger = \begin{cases} c_{n\alpha}^\dagger c_{n+1\,\alpha}^\dagger \\ (c_{n\alpha}^\dagger c_{n+1\,\beta}^\dagger - c_{n\beta}^\dagger c_{n+1\,\alpha}^\dagger)/\sqrt{2} \\ c_{n\beta}^\dagger c_{n+1\,\beta}^\dagger . \end{cases} \quad . \qquad (18)$$

A triplet bond created by $(n,n+1)_T^\dagger$ is represented by a notched arrow from n to $n+1$. The singlet operator $(n+1,n)$ annihilates any ket in which $n,n+1$ are triplet correlated, since the parallel spins cannot be transferred to a D site. Otherwise, triplet bonds satisfy many of the same relations as singlet bonds. Long triplets like $\lvert 2\rangle$ in Fig. 5, for example, are created in a manner analogous to (14):

$$(n+2,n+1)(n,n+1)^\dagger(n+2,n+3)_T^\dagger = \tfrac{1}{2}(n,n+3)_T^\dagger . \qquad (19)$$

The entire $S=1$ subspace of $-\mathcal{H}_0/\sqrt{2}\,\lvert t\rvert$ can be generated by repeatedly applying the singlet operators in (8) to the elementary triplets $\lvert 1\rangle$ and $\lvert 2\rangle$.

There is always at least one ion pair in the triplet manifold. Configuration interaction in any of the $M_s=1$, 0, or −1 subspaces leads to an absolute triplet ground state with $k=\pi$ symmetry.

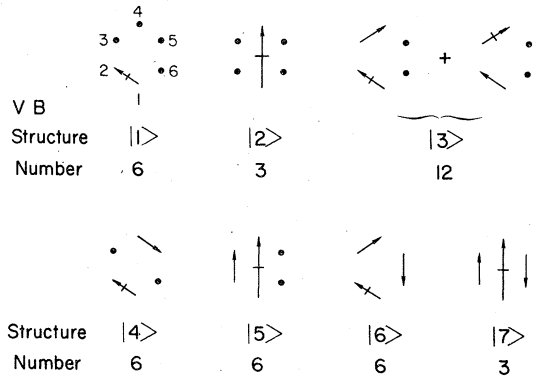

FIG. 5. Valence-bond structures in the triplet subspace of $\mathcal{H}_0$, Eq. (8), for $N=6$, with donors at odd sites and acceptors at even sites.

We again use plus (minus) phases for $(n,n+1)^\dagger$ with n odd (even). The symmetry-adapted triplet kets $|1\rangle$ and $|2\rangle$ corresponding to (13) are

$$|1\rangle = \sum_{n=1}^{6} (-1)^{n+1}(n,n+1)^\dagger_T |0\rangle ,$$
$$|2\rangle = \sum_{n=1}^{3} (-1)^{n+1}(n,n+3)^\dagger_T |0\rangle . \tag{20}$$

Operation with $h = -\mathcal{H}_0/\sqrt{2}|t|$ on the VB structures in Fig. 5 after symmetry adapting to $k=\pi$ leads to the linear equations

$$\begin{aligned}
h|1\rangle &= 2z|1\rangle + |3\rangle + |4\rangle ,\\
h|2\rangle &= 2z|2\rangle + |5\rangle ,\\
h|3\rangle &= 4z|3\rangle + 2|1\rangle + 2|2\rangle + 2|6\rangle ,\\
h|4\rangle &= 4z|4\rangle + |1\rangle ,\\
h|5\rangle &= 4z|5\rangle + |1\rangle + |2\rangle + 2|7\rangle ,\\
h|6\rangle &= 6z|6\rangle + \tfrac{3}{2}|3\rangle + \tfrac{1}{2}|5\rangle ,\\
h|7\rangle &= 6z|7\rangle + \tfrac{1}{2}|3\rangle + |5\rangle .
\end{aligned} \tag{21}$$

The operator identity

$$(n,n+1)^\dagger(n+2,n+3)^\dagger_T + (n,n+1)^\dagger_T(n+2,n+3)^\dagger = (n,n+3)^\dagger_T(n+1,n+2)^\dagger + (n,n+3)^\dagger(n+1,n+2)^\dagger_T , \tag{22}$$

can be represented diagrammatically as

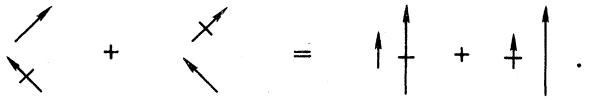

(23)

It follows that ↕↑ is linearly dependent on the VB structures retained in Fig. 5. Such identities hold quite generally provided that all four diagrams in (23) have the same arbitrary distribution of bonds at other sites. Both bonds can be long, as occurs in $N=8$ and $N=10$ diagrams, and care must be taken with phases.

Arranging the coefficients of (21) into columns leads to a nonsymmetric 7×7 matrix for any M_s component of the $\{1,\pi\}$ subspace

$$\frac{-\mathcal{H}_0}{\sqrt{2}|t|} = \begin{bmatrix}
2z & 0 & 2 & 1 & 1 & 0 & 0\\
0 & 2z & 2 & 0 & 1 & 0 & 0\\
1 & 0 & 4z & 0 & 0 & 3/2 & 1/2\\
1 & 0 & 0 & 4z & 0 & 0 & 0\\
0 & 1 & 0 & 0 & 4z & 1/2 & 1\\
0 & 0 & 2 & 0 & 0 & 6z & 0\\
0 & 0 & 0 & 0 & 2 & 0 & 6z
\end{bmatrix} . \tag{24}$$

The largest root $\lambda_{1\pi}(z)$ of (24) is again found iteratively and gives the lowest triplet energy $-\sqrt{2}|t|\lambda_{1\pi}(z)$ of $\mathcal{H}_0$. The magnetic gap ΔE_m is given by

$$\Delta E_m(z)/\sqrt{2}|t| = \lambda_0(z) - \lambda_{1\pi}(z), \tag{25}$$

where $\lambda_0(z)$ is the larger of $\lambda_{00}(z)$ and $\lambda_{0\pi}(z)$. Table III summarizes values of $\lambda_{1\pi}(z)/N$ and of $\Delta E_m(z)$ for rings of $N=4$, 6, 8, and 10. The behavior of $\Delta E_m(z,N)$ is shown in Fig. 6 and is discussed below.

Quintet states can be generated by constructing the most neutral VB structure with a pair of D^+A^- sites and subsequently applying $-\mathcal{H}_0/\sqrt{2}|t|$ repeatedly. Higher multiplicities can be treated similarly. All these states, as well as the other k sub-

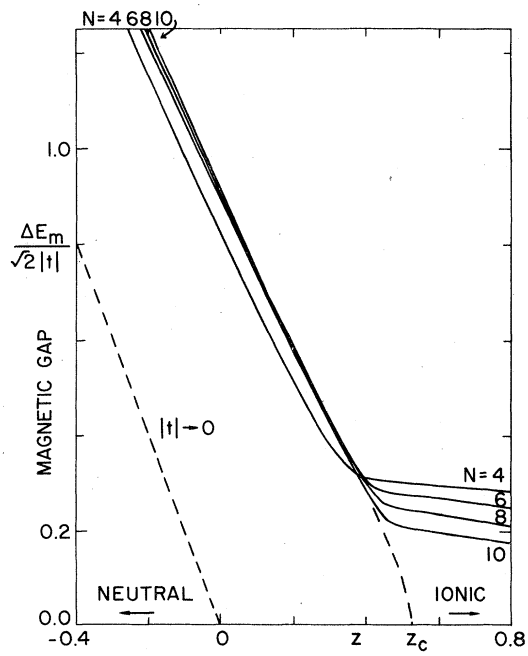

FIG. 6. Magnetic gap $\Delta E_m(z,N)/\sqrt{2}|t|$ vs z for rings of $N=4$, 6, 8, and 10 sites. The dashed line has slope -2 and gives the limit $|t|\to0$. The extrapolation to vanishing gap at z_c is discussed in the text.

TABLE III. Lowest triplet energy per site $\lambda_{1\pi}(z)/N$, in units of $-\sqrt{2}|t|$, and magnetic gap $\Delta E_m(z)/\sqrt{2}|t|$ of $\mathcal{H}_0$, Eq. (8), for rings of $N=4, 6, 8, 10$.

$z=\delta/\sqrt{2}\|t\|$		Ring size N 4	6	8	10	Extrapolation [a] ∞
0.8	$\lambda_{1\pi}/N$	1.006 206	1.053 438	1.071 226	1.079 717	1.0970
	$\Delta E_m/\sqrt{2}\|t\|$	0.283 07	0.250 59	0.211 34	0.172 54	0.000
0.4		0.667 423	0.733 470	0.759 960	0.773 434	0.8110
		0.307 95	0.304 06	0.298 13	0.285 88	0.275
0.0		0.353 553	0.450 000	0.493 063	0.516 873	0.6105
		0.821 87	0.892 60	0.908 85	0.920 39	0.943
−0.4		0.067 423	0.206 671	0.273 411	0.313 182	0.4748
		1.494 69	1.564 31	1.583 23	1.590 97	1.615
−0.8		−0.193 798	−0.002 872	0.091 395	0.147 913	0.3757
		2.199 63	2.252 42	2.263 23	2.268 22	2.272

[a] ± 0.005 for $\Delta E_m/\sqrt{2}|t|$; $\lambda_{1\pi}(z)N^{-1}$ extrapolates to $\lambda_0(z)N^{-1}$ to order N^{-1}.

spaces for $S=0$ and $S=1$ and the excited states in the $S=0,1$ and $k=0,\pi$ subspaces, are needed to construct the partition function and obtain the complete thermodynamics of $\mathcal{H}_0$. Such complete analysis is probably limited to $N \leq 6$, while selected ground-state properties like γ or ΔE_m are readily found up to $N=10$. The VB procedure thus provides a convenient and exact description of configuration interaction in any subspace of the electron-hole Hamiltonian $\mathcal{H}_0$ in (8).

III. MAGNETIC GAP AND COLLECTIVE COULOMB INTERACTIONS

We have so far considered a fixed excitation energy -2δ for producing a D^+A^- pair. The neutral-ionic interface at $\delta/\sqrt{2}|t| = z_c = 0.53 \pm 0.01$ was obtained by extrapolating the crossover $z_c(N)$ from $k=0$ to $k=\pi$ ground-state symmetry in rings of $N=4$, 6, 8, and 10. For $z<z_c$, the lattice is diamagnetic at 0 °K and has a gap $\Delta E_m(z)$ for magnetic excitation. For $z \geq z_c$, the magnetic gap vanishes and the lattice is paramagnetic, with a finite static susceptibility $\chi(T)$ at $T=0$ °K. The extrapolation in Fig. 6 of $\Delta E_m(z)$ to z_c in the limit $N \to \infty$ cannot be justified solely on the basis of the $\Delta E_m(z,N)$ computations. Since $\chi(T)$ data offer the simplest experimental test of the model, we consider the behavior of $\Delta E_m(z)$ near z_c in greater detail.

A finite magnetic gap of $|2\delta|$ occurs in the $t \to 0$ limit of a neutral lattice. For large negative z, we consequently expect $\Delta E_m/\sqrt{2}|t| = 2z$ to have a limiting slope of -2, as indicated by the dashed line in Fig. 6. The finite CT integral t does not greatly change the behavior of $\Delta E_m(z)$ for $z<z_c$, even in the region $z \sim 0$ where the band width dominates 2δ. This supports the extrapolation to $\Delta E_m(z_c)=0$, although N-dependent behavior of $\Delta E_m(z,N)$ for $z>z_c$ complicates the situation.

The difficulty is that N-dependences are inherent in the ionic lattice. It can readily be shown that for $|2\delta| \gg t$ and $|U-2\delta| \gg t$, the general electron-hole Hamiltonian $\mathcal{H}_{eh}$ in (10) reduces to a one-dimensional Heisenberg antiferromagnet

$$\mathcal{H}_{AF} = 2J_0 \sum_n \vec{s}_n \cdot \vec{s}_{n+1}. \tag{26}$$

In this limit, the lattice is ionic and the spins $\vec{s}_n = \frac{1}{2}$ at either D^+ or A^- sites are stabilized[3] via virtual CT excitations favoring antiparallel, or singlet, pairs. The kinetic exchange $J_0>0$ is

$$J_0 = t^2[(2\delta)^{-1} + (U-2\delta)^{-1}]. \tag{27}$$

The second term vanishes for $\mathcal{H}_0$, since (8) involves the $U \to \infty$ limit and excludes D^{2+} or A^{2-} sites. The regular Hubbard model, with $\epsilon_A = \epsilon_D$ in (11), reduces to $\mathcal{H}_{AF}$ in the limit $U \gg t$ and has $J_0 = 2t^2/U$. The reduction of $\mathcal{H}_0$ to $\mathcal{H}_{AF}$ is rigorous for $z \gg 1$. Griffiths[11] has computed $\chi(0)$ exactly for $\mathcal{H}_{AF}$ with $J_0>0$ and has explicitly demonstrated triplet (and higher) states with $\Delta E_m = 0$. Numerical computations for $\mathcal{H}_{AF}$ by Bonner and Fisher[12] show that ΔE_m goes approximately as N^{-1} for even N up to $N=10$, the largest rings considered. There is consequently rigorous evidence that $\Delta E_m(z)$ for the infinite chain vanishes for large positive z.

The reduction to $\mathcal{H}_{AF}$ fails for partial CT γ, where δ and t are comparable. The magnetic gap can be expected on general grounds to open up at z_c, where the ground state switches from $k=0$ to $k=\pi$. We have analyzed the related singlet-triplet gap $\Delta E'$:

$$\Delta E'(z)/\sqrt{2}|t| = \lambda_{0\pi}(z) - \lambda_{1\pi}(z) \ , \tag{28}$$

in the $k=\pi$ subspace. For $z>z_c$, $\Delta E'(z)$ reduces to $\Delta E_m(z)$, since $\lambda_{0\pi}(z)$ is then the absolute ground

state. On the neutral side, however, $\Delta E'(z)$ is smaller than $\Delta E_m(z)$, since the singlet state $\lambda_{0\pi}(z)$ is higher in energy than $\lambda_{00}(z)$. The gap $\Delta E'(z)$ represents the singlet-triplet splitting for the *same* spatial function and is expected to vanish for *both* $z \to \infty$ and $z \to -\infty$ where CT stabilization becomes ineffective. The singlet is always expected to be lower, as it affords an additional ion pair for CT stabilization, and the maximum value of $\Delta E'(z)$ is expected at $z=0$ where CT stabilization is maximized.

The $k=\pi$ subspaces for $N=4$ contain only two states for either $S=1$ or $S=0$, as shown in Table I, and yield quadratic equations for $\lambda_{0\pi}(z,4)$ and $\lambda_{00}(z,4)$. Thus we have

$$\Delta E'(z,4)/\sqrt{2}\,|t| = (z^2+3)^{1/2} - (z^2+2)^{1/2}, \qquad (29)$$

which indeed has a maximum at $z=0$, vanishes at $z \to \pm\infty$, and is always positive. We find that $\Delta E'(0,N)$ decreases with increasing N and goes as $0.75N^{-1/2}$ for $N=6$, 8, and 10. The smaller values at $\Delta E'(\pm 0.5,N)$ decrease more rapidly and can be fit to $0.67N^{-1/2}$. For large $|z|$, the decrease of $\Delta E'(\pm z,N)$ eventually follows the N^{-1} behavior of the linear Heisenberg AF. These results support the previous assertion that the magnetic gap $\Delta E_m(z)$ opens up at z_c for the infinite lattice.

We now turn to the collective effects arising from long-range, three-dimensional Coulomb interactions. The Hartree approximation indicated in (2) amounts to a γ dependence in δ. The variation of I_D or A_A for a series of complexes with *small* CT integral t is expected to produce a discontinuous charge in γ, in contrast to the smooth $\gamma(z)$ behavior in Fig. 7 found on extrapolating the $\gamma(z,N)$ curves in Fig. 3. Such collective effects depend on the extra stabilization $m=M-M_1$ in (2) arising from embedding *DA* dimers self-consistently in the partly ionic lattice.[7] In reduced units, we define $f=m/\sqrt{2}\,|t|$ and only consider $f \geq 0$, when collective long-range interactions tend to stabilize the ionic lattice. Rearranging (2) gives

$$z_0(z,f) \equiv \delta(0)/\sqrt{2}\,|t| = z - f\gamma(z), \qquad (30)$$

where z_0 is seen from (3) to depend only on the molecular difference $I_D - A_A$ if, for simplicity, we assume that the Madelung energy M, the nearest-neighbor interactions M_1, and t are comparable for several complexes. Such an interpretation of (30) is not required, however, and the basic point remains the γ dependence of δ.

The $f=0$ curve $\gamma(z)$ in Fig. 7 suffices for constructing the other $\gamma(z_0,f)$ vs z_0 curves shown. Long-range Coulomb interactions merely renormalize δ in the Hartree approximation, thus shifting from $z=\delta/\sqrt{2}\,|t|$ to z_0 in (30). For a given value of f, z, and $\gamma(z)$, we use (30) to compute z_0 and plot the result in Fig. 7 as a function of $z_0+\frac{1}{2}f$, which conveniently places the rapid change of $\gamma(z_0,f)$ in the same region for different values of f.

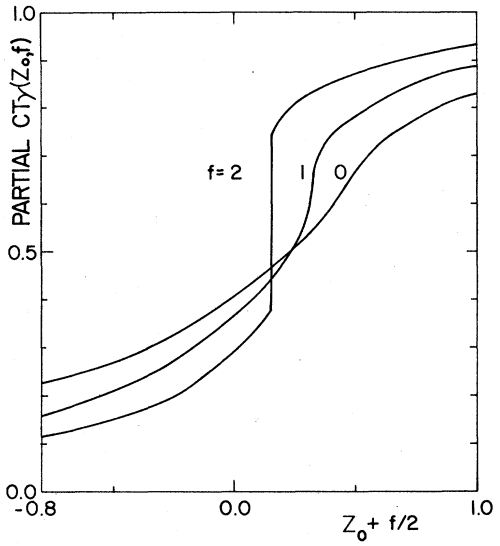

FIG. 7. Degree of CT $\gamma(z_0,f)$ vs $z_0+\frac{1}{2}f$ for collective interactions $f=m/\sqrt{2}\,|t|$ in Eq. (30). The $f=0$ curve of $\gamma(z)$ is the $N \to \infty$ extrapolation of the $\gamma(z,N)$ curves in Fig. 3. The discontinuity in $\gamma(z_0 f)$ for $f>f_c=1.4$ is discussed in the text.

Discontinuities at the neutral-ionic interface occur for $f>f_c$, when $z_0(z,f)$ is not a single-valued function of z. Since the derivative, $\gamma'(z)$, is seen in Fig. 7 to have a maximum at z_c, the first discontinuity occurs at z_c for f_c given by

$$\frac{\partial z_0}{\partial z} = 1 - f_c\gamma'(z_c) = 0. \qquad (31)$$

The value $\gamma'(z_c)=0.71\pm0.05$ is estimated from Fig. 7 or from the second t derivative of $\lambda_{00}(z)/N$ and $\lambda_{0\pi}(z)/N$. The resulting $f_c=1.4\pm0.1$ is the largest $m/\sqrt{2}\,|t|$ for which $\gamma(z_0,f)$ is continuous, with an infinite slope at $z_0(z_c,f_c)$. Any $f<f_c$, including destabilizing collective interactions leading to $f<0$, have $\gamma(z_0,f)$ smoothly varying from 0 to 1 as z_0 goes from $-\infty$ to $+\infty$. The neutral-ionic interface for $f<f_c$ is at $z_0(z_c,f_c)$. The degree of CT γ, the magnetic gap $\Delta E_m(z)$, and the ground-state symmetry previously found for $f=0$ remain unchanged for $f \leq f_c$. Small collective effects merely give more rapid variations in γ as a function of z_0.

Any $m>0$ leads to a discontinuity in $\gamma(z_0)$ in the limit $t \to 0$, in agreement with the exact result of a step function for γ when the sites do not overlap. For $f>f_c$, there are two values z_1 and $z_2>z_1$ that

satisfy (31). The larger root z_2 must be larger than z_c, since $\gamma'(z)$ decreases above z_c and thus allows a solution to (31) with $z_2 > z_c$. The ionic ground state again has $k=\pi$ symmetry. The discontinuity is $\gamma(z_2)-\gamma(z')$, where z' is defined by

$$z_0(z_2,f)=z'-f\gamma(z'). \tag{32}$$

We see from (30) and (31) that $z_0(z,f)$ decreases with increasing z between z_1 and z_2, so that $z_0(z_2,f)$ is smaller than $z_0(z_1,f)$. Now (32) leads to $z'<z_c$ since z_1 occurs at the smaller z value satisfying (31). Thus the neutral ground state at z' is clearly in the $k=0$ subspace. A curve of $\gamma(z_0,f)$ with $f>f_c=1.4$ is shown in Fig. 7. The neutral-ionic transition now occurs at

$$z_0(z_2,f)=z_2-f\gamma(z_2). \tag{33}$$

The discontinuity in the partial CT γ is $\gamma(z_2)-\gamma(z')$. The magnetic gap $\Delta E_m(z_0,f)$ and static susceptibility $\chi(T)$ vanish discontinuously, since the crossover from $k=0$ to $k=\pi$ ground states at $z_0(z_2,f)$ has a finite change in slope. The neutral-ionic interface for $f>f_c$ thus involves a first-order phase change, while the change is second order for $f\leq f_c$. As expected, collective effects can produce discontinuities on varying such single-site parameters as z_0, which depends on I_D-A_A.

IV. DISCUSSION

The motivation for more careful computations of the magnetic gap is the puzzling $\chi(T)$ behavior[3] of several strong CT complexes like $(TMPD)^{\gamma+}(TCNQ)^{\gamma-}$. Here TMPD is the π-donor NNN'N'-tetramenthyl-p-phenylenediamine and TCNQ is the π-acceptor tetracyanoquinodimethane. Infrared and optical data[13] point to an ion-radical solid, while the center of inversion at each D and A site in the crystal structure[14] requires a single CT integral t along the stack. Instead of the gapless Bonner-Fisher behavior[12] of $\chi(T)$, however, the EPR intensity[15] from 200 to 300 °K goes as

$$\chi(T)\propto e^{-\Delta E/kT}\ , \tag{34}$$

with a large magnetic gap $\Delta E\approx 0.075\pm 0.008$ eV. This clearly rules out a $\gamma\sim 1$ interpretation based on the Heisenberg AF (26), whereas the crystal structure and absence of fine-structure rule out the suggestion[16] of an alternating stack with unequal CT integrals.

The TMPD complex with the weaker acceptor chloranil also has an activated[17] $\chi(T)$, with ΔE in Eq. (34) about 0.13 eV and a crystal structure[18] with D's and A's at centers of inversion. The 1:1 complex[19] of p-phenylenediamine and chloranil also has mixed regular stacks and $\Delta E=0.13\pm 0.01$ eV between 250 and 330 °K. There is some evidence for phase transitions[16,17] at lower temperature, where in any case the inevitable occurrence[19] of mechanical defects such as "finite chains" or of chemical impurities spoils the simple exponential in (34) for $kT\ll\Delta E$.

The present results for partial CT show that a finite magnetic gap of the order of $|t|$ occurs without introducing dimerization, spin-phonon coupling, or charge-density waves. The $\Delta E_m/\sqrt{2}|t|$ results in Fig. 6 follow directly from the CT Hamiltonian $\mathcal{H}_0$ in (8). Various estimates[3] of $|t|$ in CT complexes[20] and in ion-radical crystals[21] yield $|t|\sim 0.1$ to 0.3 eV. Taking $|t|\sim 0.20$ eV ~2200 K and assuming, for the moment, that collective effects lead to $f<f_c$, we see from Fig. 7 that the TMPD-TCNQ gap of 0.075 eV implies $\Delta E_m/\sqrt{2}|t|\sim 0.25$ and $\gamma\sim 0.6$. The larger $\Delta E\sim 0.13$ eV in the weaker complexes TMPD-chloranil or phenylenediamine-chloranil give $\gamma\sim 0.5$, which is still quite ionic. A slightly larger value of $|t|$ gives higher values of the partial CT γ, although less than $\gamma_c=0.68\pm 0.01$ where $\Delta E_m\to 0$.

Several recent attempts[22-24] to catalog the various contributions[3] to the binding energies of neutral and ionic organic lattices underscore the difficulties of quantitative treatments. Thus we have lumped all differential site contributions into the term $M-(I_D-A_A)$ and all collective effects into $(M-M_1)\gamma$. Some crystal terms may not scale as γ and thus require more than a renormalization of $m=M-M_1$, which in any case represents a Hartree approximation and misses lattice relaxation,[23] various polarization contributions, and Coulomb exchange.[25] It is clear that strong donors and acceptors in mixed stacks satisfy[6] the inequality $M>I_D-A_A$ leading to an ionic lattice and that the crystal stabilization per pair, $m=M-M_1$, is given by $m\lesssim 1$ eV. Again taking $\sqrt{2}|t|\sim 0.3$ eV. we see that $f=m/\sqrt{2}|t|$ can easily be of the order of 1–3, quite possibly exceeding $f_c=1.4\pm 0.1$. Now Fig. 7 shows that the degree of CT changes discontinuously from the diamagnetic region with finite ΔE_m to the paramagnetic regime with $\Delta E_m=0$. For $f>f_c$, there is less charge transfer in the region of finite ΔE_m. In view of the uncertainties in the model parameters, in the Hartree approximation for collective interactions, and in the absence of discontinuous neutral-ionic transitions, it is premature to go beyond the observation that ΔE_m slightly smaller than $|t|$ is quite consistent with $\gamma\sim 0.4$–0.6 in mixed regular CT crystals. The application of pressure, which should increase $|t|$ more rapidly than the other parameters, may clarify whether borderline complexes undergo continuous or discontinuous neutral-ionic transitions.

1:1 CT complexes of NN'- substituted phena-

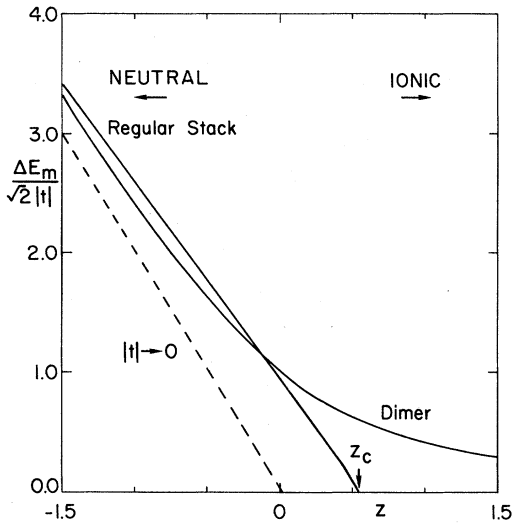

FIG. 8. Magnetic gap $\Delta E_m(z)/\sqrt{2}\,|t|$ for: the regular stack, based on $N\to\infty$ extrapolations from Fig. 6, the isolated dimer, Eq. (35), and the $|t|\to$ limit of no CT stabilization.

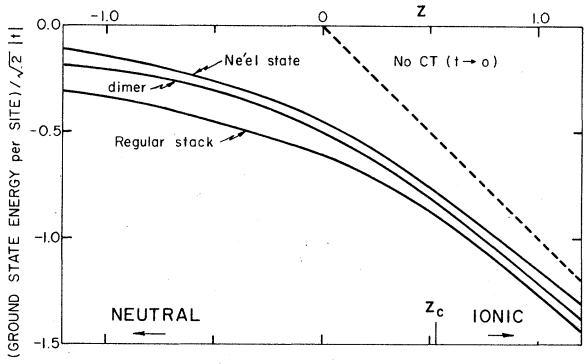

FIG. 9. Ground-state energy per site, in units of $\sqrt{2}\,|t|$, relative to the neutral vacuum state for: the regular stack, based partly on $N\to\infty$ extrapolation in Table II, the isolated dimer Eq. (36), the Néel state approximation, Eq. (38) of spinless D^+ and A^- sites and the $|t|\to 0$ limit of no CT stabilization.

zines and TCNQ span the neutral-ionic interface.[7,26] The infrared[26] and EPR (Ref. 27) of the hydromethylphenazine (HMP) complex is characteristic[3] of mixed ion-radical stacks. The dimethylphenazine complex is largely neutral at 300 K and is the first CT complex to show triplet spin-exciton splittings.[28] Both HMP-TCNQ and dimethylphenazine-TCNQ crystallize[29,30] in mixed *alternating* stacks, with different CT integrals $\ldots t_1t_2t_1t_2\ldots$ between successive DA sites. The limit $t_1 \gg t_2$ corresponds to isolated dimers and can be treated self-consistently,[7] while the opposite limit $t_1 = t_2$ has been considered in this paper. The magnetic gap for an isolated dimer (with $t_1 = t$ and $t_2 = 0$) is

$$\Delta E_d(z)/\sqrt{2}\,|t| = (z^2+1)^{1/2} - z. \tag{35}$$

As shown in Fig. 8, $\Delta E_d(z)$ and $\Delta E_m(z)$ for $t_1 = t_2 = t$ are quite similar on the neutral side of negative z, where $\Delta E/\sqrt{2}\,|t|$ vs z has a slope of -2 in the limit $|t|\to 0$. Thus turning on t_2 from $t_2 = 0$ to $t_2 = t$ in a mixed alternating stack hardly changes the magnetic gap for $z < z_c$. There is a qualitative change for $z > z_c$, where the dimer has a finite gap and the mixed regular stack has no gap. Thus we can use either limit in Fig. 8 to discuss the magnetic gap[28] $\Delta E = 0.60 \pm 0.10$ eV in dimethylphenazine-TCNQ between ~270 and 370 K. Again taking the stronger, intradimer, CT integral as $\sqrt{2}\,|t_1| \sim 0.3$ eV, we find $z \sim -0.7$ and the partial CT to be $\gamma \lesssim 0.2$. The system is indeed largely neutral.

The similarity of ΔE_m in Fig. 8 for the regular lattice $\mathcal{H}_0$ in (8) and for isolated dimers with the same $t_1 = |t|$ also shows up in the ground-state energy per site. For dimers, we have

$$\lambda_d(z) = \tfrac{1}{2}[(z^2+1)^{1/2} + z] \tag{36}$$

for the singlet ground-state energy per site, in units of $-\sqrt{2}\,|t|$. The ground-state energy $\lambda_{00}(z)/N$ or $\lambda_{0\lambda}(z)/N$ for the regular lattice is given in Table II for various rings, including $N\to\infty$ extrapolations. The results for the dimer and the regular stack are compared in Fig. 9. Changing t_2 from 0 in the dimer to $|t|$ in the regular chain is again seen to be a relatively small effect. Figure 9 also shows the ground-state energy per site $\lambda_N(z)/N$ for the approximation to $\mathcal{H}_0$ with *spinless* D^+ or A^- sites,

$$\mathcal{H}_N = -|t|\left(\sqrt{2z}\sum_n f_n^\dagger f_n + \sum_n (f_n^\dagger f_{n+1}^\dagger + f_{n+1} f_n)\right). \tag{37}$$

Here $f_n^\dagger, f_n$ are the Fermion operators $c_{n\beta}^\dagger, c_{n\beta}$ for even n and $c_{n\alpha}^\dagger, c_{n\alpha}$ for odd n. This amounts[7] to restricting the CT excitations of $\mathcal{H}_0$ to having β spins at odd, or D, sites and α spins at even, or A, sites. The corresponding ionic lattice resembles the Néel state $\ldots D^+\beta A^-\alpha D^+\beta A^-\alpha\ldots$. This model was introduced by Krugler, Montgomery, and McConnell[31] in the first discussion of the neutral-ionic interface. Although $\mathcal{H}_N$ spoils the magnetic properties by suppressing the spin degeneracy of the ion-radicals, it has the important virtue of being exactly soluble.[31,32] The ground-state energy per site in units of $-\sqrt{2}\,|t|$ and degree of CT are, respectively,

$$\begin{aligned} \lambda_N(z)/N &= \sqrt{2}\,E(m)/\pi m + \tfrac{1}{2}z, \\ \gamma_N(z) &= \tfrac{1}{2}[1 + zmK(m)/\sqrt{2\pi}], \end{aligned} \tag{38}$$

where $m^2 = 2/(2+z^2)$ and $K(m), E(m)$ are complete elliptic integrals of the first and second kind. The first point is that $-\lambda_N(z)/N$ in Fig. 9 is seen to be a poorer approximation than $-\lambda_d(z)/N$, so that the simple dimer limit is preferable[7] to the Néel state. The second point is that $\gamma_N(z)$ clearly reduces to $\gamma_N(0) = \frac{1}{2}$ and is symmetric about $z = 0$, thus confirming that the asymmetry of $\gamma(z)$ in Fig. 3 has to do with the spin degeneracy of $A^-\sigma$ and $D^+\sigma$.

It should be noted that the $\gamma \to 1$ limit of alternating stacks reduces to the alternating[33] Heisenberg AF, which has a magnetic gap that reduces to J_0 in (27) in the limit of isolated dimers. However, $\Delta E_m \sim 0.6$ eV requires $|t| \gtrsim 1$ eV in either (27) or (35) if an ionic lattice with $z \gg 1$ is postulated. Thus it is the magnitude, rather than the occurrence, of ΔE_m that suggests a largely neutral ground state for dimethylphenazine-TCNQ. The absence of hyperfine structure in the triplet spin-exciton spectra[28] then shows that dimethylphenazine-TCNQ does not correspond to isolated triplets, but has mobile triplet states with unpaired electrons on adjacent D^+ and A^- ion-radicals. Resolved fine structure remains the simplest magnetic feature of alternating chains.

We have discussed room-temperature $\chi(T)$ data in terms of purely ground-state properties. The thermodynamics of $\mathcal{H}_0$ can, of course, be found explicitly for small ring $N \simeq 6$, as pointed out in Sec. II. For large magnetic gap $\Delta E_m \gg kT$, as is the case for the CT complexes considered, the thermal equilibrium population of excited states is quite low. Ground-state results then suffice. Indeed, it is likely that lower-temperature results are dominated by mechanical or chemical impurities even in carefully prepared samples. The description of systems with $\Delta E_m = 0$, by contrast, requires a more complete knowledge of the energy spectrum of $\mathcal{H}_0$.

The most striking property[26] of dimethylphenazine-TCNQ is the reversible onset of paramagnetism above 370 °K, where the triplet spin-exciton fine-structure collapses.[28] The rather small value of $\gamma \sim 0.2$ suggested by the large magnetic gap is, in fact, smaller than expected if there is to be a neutral-ion transition around 370 °K. Further conducitivity and single crystal EPR experiments are in progress to clarify the high-temperature behavior of dimethylphenazine-TCNQ. The present theoretical work on the neutral-ionic interface has primarily focused on developing the first rigorous model for intermediate γ and for the behavior of ΔE_m. The model provides a consistent picture for the neutral-ionic interface, but it may not be complete enough for real CT complexes.

The CT Hamiltonian (8) also describes CT excitations and conducting states. We have deliberately omitted these. CT excitations involve higher energies in the $S = 0, k = 0$ subspaces and thus require going beyond the rapid iterative procedure for finding the ground state in any $\{S, k\}$ subspace. Conducting states are expected in subspaces with degenerate wavevector k in (9). Transport properties probably will require explicit consideration of both intramolecular and lattice phonons, as well as more accurate treatment of the Coulomb interactions. As has already been emphasized in connection with the deferred thermodynamics of $\mathcal{H}_0$, we have concentrated on two ground-state properties, the degree of CT $\gamma(z)$ and the magnetic gap $\Delta E_m(z)$, for arbitrary values of $z = \delta/\sqrt{2}|t|$ when D^{2+} and A^{2-} sites are excluded. Both $\gamma(z)$ and $\Delta E_m(z)$ have been computed for finite rings of $N = 4, 6, 8, 10$ and extrapolated to $N \to \infty$ by a novel application of VB techniques.

Note added in proof. Resonance Raman[34] on TCNQ vibrations shows that $TMPD^{+\gamma}TCNQ^{-\gamma}$ is less than completely ionic, with $\gamma \sim 0.7$, in good agreement with theory.

ACKNOWLEDGMENTS

It is a pleasure to thank T. T. P. Cheung, D. J. Klein, and T. M. Rice for a number of stimulating discussions and suggestions. This work was supported by NSF Grant No. CHE76-07377.

[1] H. M. McConnell, B. M. Hoffman, and R. M. Metzger, Proc. Natl. Acad. Sci. USA 53, 46 (1965); P. L. Nordio, Z. G. Soos, and H. M. McConnell, Annu. Rev. Phys. Chem. 17, 237 (1966).

[2] D. J. Klein and Z. G. Soos, Mol. Phys. 20, 1013 (1971).

[3] Z. G. Soos, Annu. Rev. Phys. 25, 121 (1974); Z. G. Soos and D. J. Klein in *Molecular Association*, edited by R. Foster (Academic, New York, 1975), Vol. 1, pp. 1–109. These reviews summarize the experimental data and literature on Solid CT complexes.

[4] P. J. Strebel and Z. G. Soos, J. Chem. Phys. 53, 4077 (1970).

[5] Z. G. Soos and S. Mazumdar, Chem. Phys. Lett. (to be published) contains a preliminary report.

[6] R. M. Metzger, J. Chem. Phys. 57, 1876 (1972).

[7] Z. G. Soos, H. J. Keller, W. Moroni, and D. Nöthe, Ann. N.Y. Acad. Sci. (to be published).

[8] L. Pauling, J. Chem. Phys. 1, 280 (1933); G. Rumer, Nachrichten technik 1932, 377 (1932); H. Eyring, J. Walter, and G. E. Kimball, *Quantum Chemistry* (Wiley, New York, 1944), Chap. XIII; G. W. Wheland, *Resonance in Organic Chemistry* (Wiley, New York,

1955), Chap. 9.
[9]V. Y. Krivnov and A. A. Ovchinnikov, Sov. Phys. Solid State 15, 118 (1973).
[10]N. Gastinel, *Linear Numerical Analysis* (Academic, New York, 1970), pp. 314–318.
[11]R. B. Griffiths, Phys. Rev. 133, A768 (1964).
[12]J. C. Bonner and M. E. Fisher, Phys. Rev. 135, A640 (1964).
[13]R. Foster and T. J. Thomson, Trans. Far. Soc. 59, 269 (1963); H. Kuroda, S. Hiroma, and H. Akamatu, Bull. Chem. Soc. Jpn. 41, 1998 (1968).
[14]A. W. Hanson, Acta. Crystallogr. 19, 610 (1965).
[15]M. Kinoshita and H. Akamatu, Nature 207, 291 (1965); B. M. Hoffman and R. C. Hughes, J. Chem. Phys. 52, 4011 (1970); M. Ohmasa, M. Kinoshita, M. Sano, and H. Akamatu, Bull. Chem. Soc. Jpn. 41, 1988 (1968).
[16]S. Stemad and E. Ehrenfreund, AIP Conf. Proc. 18, 1499 (1972).
[17]G. T. Pott and J. Kommandeur, Mol. Phys. 13, 373 (1967); T. Z. Huang, R. P. Taylor, and Z. G. Soos, Phys. Rev. Lett. 28, 1054 (1972).
[18]J. L. De Boer and A. Vos, Acta Crystallogr. B 24, 720 (1967).
[19]R. C. Hughes and Z. G. Soos, J. Chem. Phys. 48, 1066 (1968).
[20]R. S. Mulliken and W. R. Person, *Molecular Complexes: A Lecture and Reprint Volume* (Wiley, New York, 1969), p. 127.
[21]J. Tanaka, M. Tanaka, T. Kawai, T. Takabe, and O. Maki, Bull. Chem. Soc. Jpn. 49, 2358 (1976); A. J. Berlinsky, J. F. Carolan, and L. Weiler, Solid State Commun. 15, 795 (1974).
[22]R. M. Metzger and A. N. Bloch, J. Chem. Phys. 63, 5098 (1975); R. M. Metzger, Proc. N.Y. Acad. Sci. (to be published).
[23]A. J. Epstein, N. O. Lipari, D. J. Sandman, and P. Nielsen, Phys. Rev. B 13, 1569 (1976).
[24]V. E. Klymenko, V. Y. Krivnov, A. A. Ovchinnikov, I. I. Ukrainsky, and A. Shvets, Sov. Phys. JETP 42, 123 (1975).
[25]Z. G. Soos and A. J. Silverstein, Mol. Phys. 23, 775 (1972).
[26]Z. G. Soos, H. J. Keller, W. Moroni, and D. Nöthe, J. Chem. Soc. 99, 5040 (1977).
[27]R. C. Hughes (private communication).
[28]D. Nöthe, W. Moroni, H. J. Keller, Z. G. Soos, and S. Mazumdar, Solid State Commun. (to be published).
[29]B. Morosin, Acta. Crystallogr. (to be published).
[30]I. Goldberg and U. Shmuel, Acta. Crystallogr. B 29, 440 (1973).
[31]J. I. Krugler, C. G. Montgomery, and H. M. McConnell, J. Chem. Phys. 41, 2421 (1964).
[32]S. Katsura, Phys. Rev. Lett. 127, 1508 (1962); E. H. Lieb, T. D. Schultz, and D. C. Mattis, Ann. Phys. (N.Y.) 16, 407 (1961).
[33]L. N. Bulaevskii, Sov. Phys.-Solid State 11, 921 (1969); Z. G. Soos, J. Chem. Phys. 43, 1121 (1965).
[34]R. P. Van Duyne (private communication); M. R. Suchanski, Ph.D. thesis (Northwestern University, 1977) (unpublished).